doi:10.1016/j.jmb.2009.07.083 J. Mol. Biol. (2009) 394, 383–390

JMB

Available online at www.sciencedirect.com

ScienceDirect

ELSEVIER

Single-Molecule Force Spectroscopy Measures Structural Changes Induced by Light Activation and Transducer Binding in Sensory Rhodopsin II

Leoni Oberbarnscheidt[1], Richard Janissen[1], Swetlana Martell[2], Martin Engelhard[2] and Filipp Oesterhelt[1]*

[1]*Institut für molekulare physikalische Chemie, Universitätsstr. 1, 40225 Düsseldorf, Germany*

[2]*Max-Planck-Institut für molekulare Physiologie, Otto-Hahn-Str. 11, 44227 Dortmund, Germany*

Received 27 May 2009; received in revised form 27 July 2009; accepted 28 July 2009
Available online 3 August 2009

Edited by R. Huber

Microbial rhodopsins are a family of seven-helical transmembrane proteins containing retinal as chromophore. Sensory rhodopsin II (SRII) triggers two very different responses upon light excitation, depending on the presence or the absence of its cognate transducer HtrII: Whereas light activation of the *Np*SRII/*Np*HtrII complex activates a signalling cascade that initiates the photophobic response, *Np*SRII alone acts as a proton pump.

Using single-molecule force spectroscopy, we analysed the stability of *Np*SRII and its complex with the transducer in the dark and under illumination. By improving force spectroscopic data analysis, we were able to reveal the localisation of occurring forces within the protein chain with a resolution of about six amino acids. Distinct regions in helices G and F were affected differently, depending on the experimental conditions. The results are generally in line with previous data on the molecular stability of *Np*SRII. Interestingly, new interaction sites were identified upon light activation, whose functional importance is discussed in detail.

Keywords: sensory rhodopsin; atomic force microscopy; single-molecule force spectroscopy; membrane protein complex; protein unfolding

Introduction

Sensory rhodopsin II (SRII) is a member of the large family of microbial rhodopsins.[1,2] These type 1 rhodopsins are seven-α-helical transmembrane proteins that occur in all three domains of life. An all-*trans*-retinal covalently bound to the middle of the seventh helix absorbs light, and its resulting isomerisation to the 13-*cis* form induces different responses such as ion-pumping activity by bacteriorhodopsin and halorhodopsin or mediation of the phototactic response of sensory rhodopsins SRI and SRII in halophilic archaea in order to trigger phototaxis.

In microbial rhodopsins, the process of light activation includes the isomerisation of the retinal and rearrangements in the active site, finally leading to an outward movement of helix F.[2,3] The excitation, isomerisation and return to the all-trans state of retinal are organised in a photocycle comprising several intermediate states named K, L, M1, M2, N and O, which had been first described for the BR photocycle.[2,4,5] Complex conformational changes (especially of helix F) during the second part of the photocycle, which open the cytoplasmic channel and change the accessibility of the active side to enable ion pumping, have been described.[6]

Interestingly, *Np*SRII from *Natromonas pharaonis* has two distinct functions, depending on the presence of its cognate transducer *Np*HtrII. In the absence of the transducer, *Np*SRII acts as a proton pump,[7,8] although weaker than that of bacteriorhodopsin. In order to mediate phototaxis, *Np*SRII binds tightly to *Np*HtrII, which then activates a signalling cascade homologous to the two-component system of eubacterial chemotaxis.[9,10] The transducer consists of a transmembrane domain of two α-helices (TM1 and TM2), which binds to the receptor, and a large cytoplasmic domain, which is responsible for signal transfer.[3,11] Certain residues in helices F and G were identified to be crucial for both, transducer

*Corresponding author. E-mail address: Filipp.Oesterhelt@uni-duesseldorf.de.

Abbreviations used: SRII, sensory rhodopsin II; SMFS, single-molecule force spectroscopy; AFM, atomic force microscopy; WLC, worm-like chain; EPR, electron paramagnetic resonance; FRET, fluorescence resonance energy transfer.

binding and signal transfer.[12] However, there remain open questions and contradictory arguments about the exact movement of helix F, the possible involvement of a helix G movement and the precise molecular influence between SRII and its transducer.

We performed single-molecule force spectroscopy (SMFS) measurements on *Np*SRII, in the presence and in the absence of *Np*HtrII, and compared them to measurements in its inactive state in the dark and in the illuminated state. *Np*SRII is stable in dark and light, and it retains its native absorption spectrum and photocycle in different membranes.[13] We used the truncated form of the transducer $HtrII_{114}$, which allowed us to minimise the unwanted interaction of the transducer with the atomic force microscope (AFM) tip. This form lacks most of its cytoplasmic domain but interacts with *Np*SRII and is shown to be functional *in vitro*.[14]

In a previous SMFS study, unfolding of *Np*SRII has revealed a pattern similar to that observed in other archaeal rhodopsins[15–17] and has shown that binding of the transducer stabilises helices G and F. Here we present changes in stability upon light activation and their dependency on the presence of the transducer, which were obtained by an optimised SMFS data analysis. By taking the changes in the probability of peak occurrence as a measure for changes in protein stability, we are able to detect and localise structural changes that alter intramolecular and intermolecular bonds.

Results

SMFS of *Np*SRII

We determined the light-dependent reorganisation of interactions that stabilise structural regions of *Np*SRII and *Np*SRII bound to a truncated form of its transducer ($NpHtrII_{114}$) by applying SMFS, as described previously for *Np*SRII and other archaeal rhodopsins.[15–17] Briefly, force–distance measurements were performed on membrane patches with reconstituted *Np*SRII or *Np*SRII/*Np*HtrII, which were adsorbed on mica support. The tip was pushed into the membrane to allow an unspecific interaction between the tip and the C-terminus of the protein (as previously described by Oesterhelt *et al.*[15] and Muller *et al.*[18]). Retraction of the tip led to sequential unfolding of *Np*SRII, which was recorded by detecting the bending of the cantilever. For each force curve, the sample was shifted by 10 nm to ensure that *Np*SRII was always unfolded from an unperturbed part of the membrane. Force–distance traces showing successful unfolding were selected as described by Cisneros *et al.*[17]

The experiments were conducted first in the dark and then under exposure to blue light ($\lambda = 460$–500 nm). The intensity was chosen such that saturation occurs and about 25% of *Np*SRII is in its activated state (passing the M to O state).[2] A total of 103 and 87 force–distance curves for *Np*SRII alone and 94 and 103 force–distance curves for the *Np*SRII/$NpHtrII_{114}$ complex were collected in the dark and under blue light, respectively. The probability of peak occurrence in each data set was analysed separately and then compared to the others.

Peak positions reflect the localisation of intermolecular and intramolecular interactions

An overlay of the force curves shows the characteristic pattern of four main peaks (Fig. 1a), as already described for rhodopsins[15,19] and sensory rhodopsin in particular:[17] Each main peak represents the unfolding of an α-helix pair pulled out from the cytoplasmic side.[15] Additionally, most force curves reveal further side peaks representing unfolding intermediates and alternative unfolding pathways (Fig. 1b) that differ depending on the experimental condition.[16–19]

Each force peak detected an individual force–distance curve was fitted using the worm-like chain (WLC) model with a fixed persistence length of 0.4 nm, which is known to fit an unfolded amino acid chain[18] well above 50 pN. The contour length, as derived from the WLC fit, can be converted into the number of stretched amino acids, giving the unfolded portion of the polypeptide chain and thus elucidates the remaining intermediate structure.

However, the contour length derived from the WLC fit only reflects that part of the unfolded peptide chain that ranges from the tip to the upper surface of the membrane and neglects the part inside the membrane.[15,18] If rupture occurs inside the membrane, we have to correct for the complete chain length and thus calculate the expected measured lengths for all amino acids according to their *z*-positions in the crystal structure (Protein Data Bank ID 1H2S).[20]

Average shifted histograms with varying bin widths allow higher resolution in peak occurrence probabilities

To visualise the peak occurrence probabilities, the fitted rupture lengths are usually displayed as standard histograms. However, the shape of standard histograms significantly depends on the bin width and the chosen starting point, especially at an overall low number of counts. To avoid artefacts due to an arbitrarily chosen starting point and to accurately reflect the density of rupture lengths measured with SMFS, we displayed the rupture lengths data as an average shifted histogram.[21] In the case of monomodal data distribution, an optimal histogram bin width may be calculated from the standard deviation of the data.[22–24] However, the length distributions obtained from protein unfolding experiments are always multimodal. Thus, we extended the average shifted histogram to variable bin widths that were selected such that 20 events were collected per bin. This kept noise at a level that allowed the comparison of various data sets also at rupture lengths where only a low number of events were detected. The heights of the histogram bins in

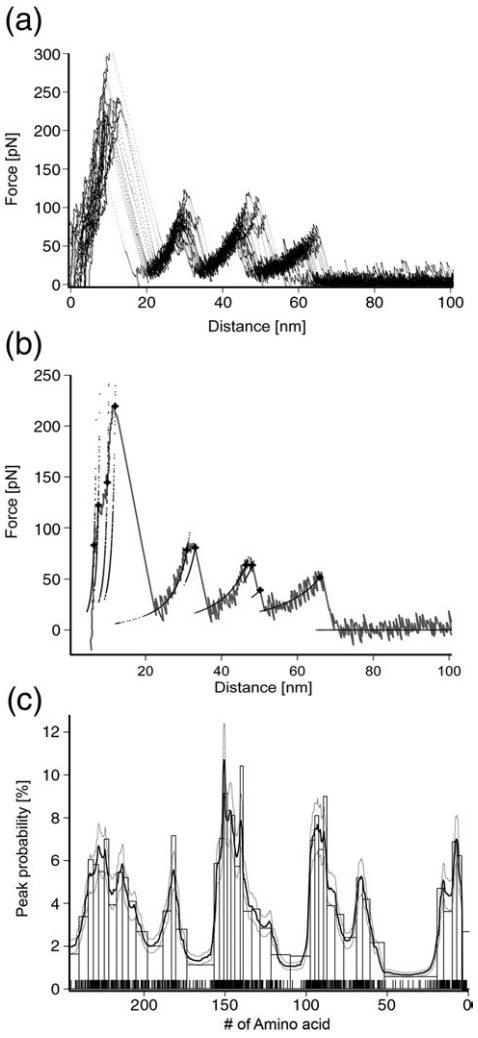

Fig. 1. Illustration of the force curve analysis procedure. (a) Overlaid force curves measured on *Np*SRII alone in the dark. The data are displayed as a dot plot. (b) Single force curve. The rupture force peaks (crosses) were detected by searching for minima in the smoothed derivative of the force curve. The left-hand sides of the force peaks were fitted with the WLC model (dotted black line) (monomer length = 3.6 Å; persistence length = 4.0 Å) to obtain the corresponding chain lengths. (c) Histogram showing the peak frequency of the monomer lengths derived from the WLC fit (bars; 1 bar = 20 events). An "average shifted histogram," which is created by shifting the starting point of the binnings in steps of one (black line), is overlaid. The errors were estimated by assuming a Poisson distribution (dotted black line). Raw data (i.e., individual fitted chain lengths of the rupture event) are shown as sticks below the histogram.

Fig. 1c were calculated such that the area of each bin was normalised to the constant number of 20 counts per bin.

To estimate the errors of a given number of force peaks at a fixed length the standard deviation of the respective probability distribution was calculated. With the assumption of a fixed probability to detect an unfolding event of a length within a given range, the probability to obtain any number of events from the whole data set is given by a Poisson distribution. Therefore, the error bars can be estimated as the square root of the number of detected events per bin (estimated error limits in Fig. 1c).

The force peak histograms (Fig. 1c) show the typical pattern of the unfolding of archaeal rhodopsins, as previously described by Cisneros *et al.*[17] The unfolding of an α-helix pair can be traced in the four main peaks. Additionally, the average shifted histograms give a more detailed picture of the unfolding of smaller substructures, which is revealed in multisubpeaks.

SMFS reveals manifold changes of interactions in helices F and G upon light excitation

To quantify the change in peak probability between the four experimental conditions, we calculated the difference curves between *Np*SRII and *Np*SRII/*Np*HtrII, between *Np*SRII and *Np*SRII$_{light}$, and between *Np*SRII/*Np*HtrII and *Np*SRII/*Np*HtrII$_{light}$ (Fig. 2a–c, lower curves) after having normalised each average shifted histogram on the respective number of measured force curves.

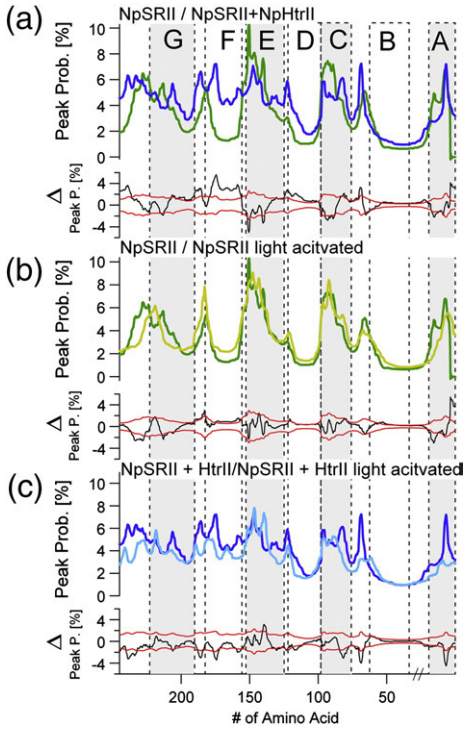

Fig. 2. Peak occurrence probabilities for the unfolding of *Np*SRII. (a) Comparison of the unfolding of *Np*SRII alone (green) and in complex with its transducer *Np*HtrII (blue). (b) Comparing the unfolding of *Np*SRII in dark (dark green) and in the light-activated state (light green). (c) Comparing the unfolding of the *Np*SRII/*Np*HtrII complex in the dark (dark blue) and in the light-activated state (light blue). Under the curves, the differences of the respective peak occurrence probabilities are plotted as black lines, whereas the estimated errors of the curves are shown in red. The vertical dotted lines indicate the range of transmembrane α-helices (Protein Data Bank ID 1H2S).

Since both data sets have errors, 1σ errors (68.3%) for comparing the two data sets (estimated error limits in Figs. 2 and 3) can be calculated by error propagation as the square root of the sum of both squared standard deviations. They give the error limits above or below which changes in the peak occurrence frequency between the different data sets may be regarded as significant, indicating a structural change in the protein.

Under all four experimental conditions, *Np*SRII exhibits different probabilities for force peak detection (Fig. 2). As already known from SMFS experiments on other α-helical membrane proteins in the absence of the transducer, the strongest peak occurrence probability is observed at the onset of the helices with respect to the pulling direction. This is changed upon transducer binding, where an increase in the peak occurrence probability is observed in the second half of the helices, reflecting a stabilising effect of the transducer. Also, light activation shows distinct changes in stabilising interactions. However, they are smaller than those induced upon transducer binding, which may also be due to the fact that only about 25% of illuminated proteins are in their activated state. Interestingly, light-induced changes observed in the presence of the transducer are stronger than those observed in its absence.

Of special interest are the first peaks, which reflect structural changes occurring in helices F and G, since these are involved in both, transducer binding and formation of the intramolecular hydrogen bond network, which plays an important role in proton transfer in the absence of the transducer.[2] The superposition of peak probability histograms for helices G and F is shown in Fig. 3 and reveals similarities and differences between all four data sets: Light activation and transducer binding, in *Np*SRII alone and in complex, lead to a decrease in rupture events in helix G (Fig. 3, region 2) and in the C-terminus. Regarding the receptor alone, light activation and transducer binding lead to a decrease in the middle of helix G (Fig. 3, region 1) and an increase in the loop region (Fig. 3, region 4). The only region where changes occur upon *Np*HtrII binding but not upon light activation is the extracellular part of helix G (Fig. 3a, region 3), where the peak probability decreases. While almost no rupture event was measured in helix F in the absence of the transducer, rupture events occurred almost as frequently as in the extracellular side of helix G in the presence of the transducer (Fig. 3, region 5). However, upon light activation, the number of rupture events again decreases in regions of helix F (Fig. 3, regions 5A and 5B). Altogether, these results reveal complex changes in localised stabilising interactions upon

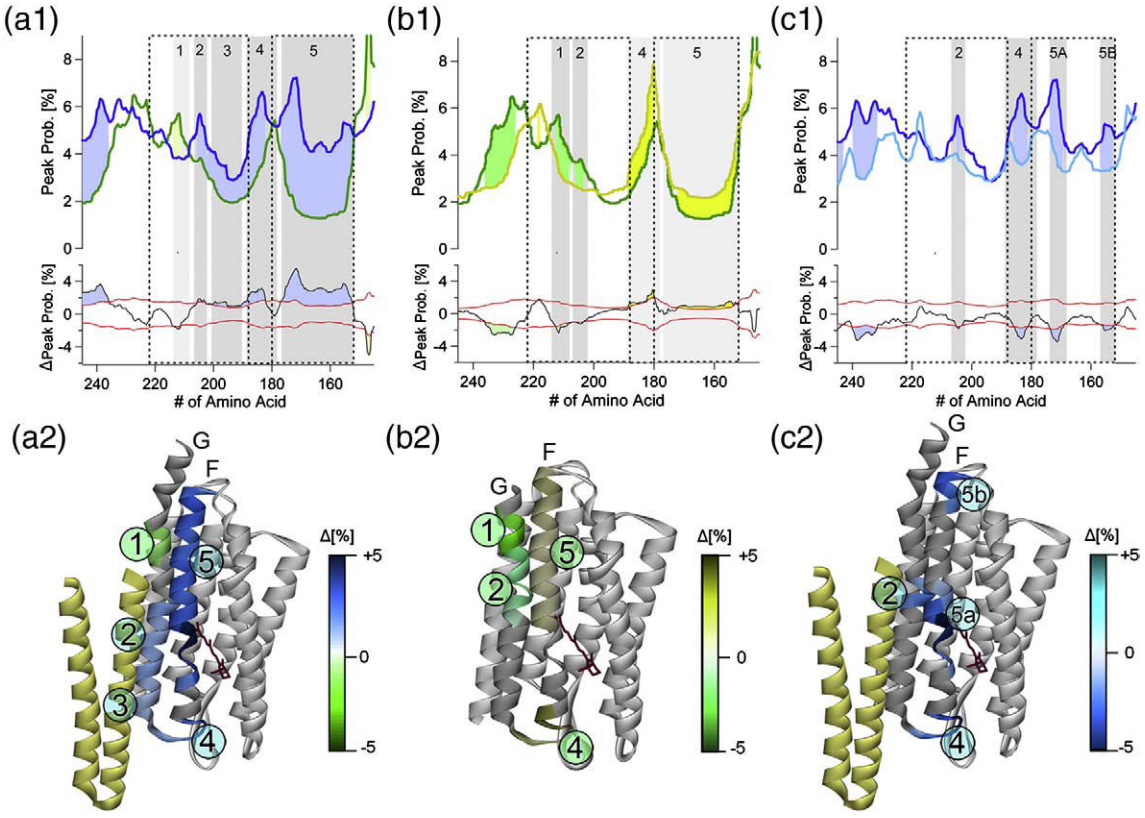

Fig. 3. Zoom to the peak occurrence probabilities in helices G and F. (a1–c1) A zoom to the peak occurrence probabilities in helices G and F, as shown in Fig. 2 (same colour code used). (a2–c2) The respective localisation of significant changes in the crystal structure (Protein Data Bank ID 1H2S). The colour code next to the crystal structure indicates the strength of the change in stabilisation of the respective regions.

light activation, which are again modulated by the presence of the transducer.

Discussion

Advanced SMFS data analysis

*Np*SRII has already been well studied, but there remain some open questions concerning the tilt of helix F and details about the signal transfer between receptor and transducer (reviewed by Klare *et al.*[2]). In contrast to many techniques which require *Np*SRII to be in solution to investigate its structure–function relationship, we are able to study the interactions of wild-type *Np*SRII inside the membrane using AFM. Thus, we avoid artefacts due to the influence of artificial solubilisation.[25]

Former AFM studies on membrane proteins, especially rhodopsins, revealed their unfolding pathways from which a high level of homology of their structural elements could be concluded.[15,18] As previously shown, the unfolding pattern of *Np*SRII is similar to those of other archaeal rhodopsins.[17] In this previous study, ensemble averaged forces were calculated by multiplying the frequency of rupture events with their respective rupture forces, revealing a partial stabilisation of helices G and F upon transducer binding. Here, we present changes upon light activation and introduce an improved force curve analysis (which allows us to achieve a more detailed view of the interaction pattern alone from the rupture frequency) not requiring ensemble average calculation.

As known from the crystal structure,[20] helices G and F are in close proximity to *Np*HtrII. Thus, in our analysis, we concentrated on changes in the stability of helices F and G, which reflect direct interactions with the transducer. By applying our data analysis procedure to the SRII unfolding data, we could reveal five different regions within helices G and F which responded independently to transducer binding and light induction.

Conformational answer after light activation varies with transducer binding

Upon transducer binding, we observe a loss of stabilising interactions in the cytoplasmic half of helix G (Fig. 3a, region 1; Table 1). In contrast, stabilisation is found in the F-G loop (region 4), the extracellular half of helix G (regions 2 and 3) and throughout helix F (region 5). A comparison with crystallographic data[20] reveals that the hydrogen bonds between *Np*SRII and *Np*HtrII existing in these regions may contribute to the observed stabilisations. Thr189 (end of F-G loop) is reported to bind to Glu43 (TM1) and Ser62 (TM2), and Tyr199 (extracellular half of helix G) is reported to bind to Asn74 (TM2). In addition, electron paramagnetic resonance (EPR), isothermal titration calorimetry and fluorescence resonance energy transfer (FRET)[26–28] revealed an interaction of the cytoplasmic side of helix F with the cytoplasmic extension of the transducer, which was not resolved in the crystal structure.

The regions identified here only on the basis of the peak occurrence probability necessarily differ from those identified on the basis of calculated ensemble forces.[17] The probability of peak occurrence, which reflects the probability that a specific interaction exists at the distinct moment, depends on the corresponding on-rate and off-rate. In contrast, the measured forces depend on the off-rate and the width of the binding potential and thus reflect different characteristics of molecular interactions.

To address the molecular changes upon light activation, we compare the light-induced stabilisation or destabilisation of the protein depending on the presence and the absence of the transducer. We find changes in stability that are independent of transducer binding, as well as those that are dependent on it.

Independent of *Np*HtrII binding, light activation always decreases the molecular stability in region 2 in the middle of helix G. This region harbours the retinal-binding site and includes amino acids Lys205 and Asp201, which form hydrogen bonds with the central water cluster, as shown by the crystal structure of the *Np*SRII/*Np*HtrII complex.[29] The structure of the M state revealed that these bonds are broken upon light excitation. This is in good agreement with the decrease in stability observed for this region.

In contrast, in all other regions, conformational changes upon light activation are modulated by the binding of the transducer. In the cytoplasmic half of helix G (region 1), light activation induces destabilisation of *Np*SRII alone, while no change is observed in the *Np*SRII/*Np*HtrII complex. Considering the literature, quite contradictory results are presented for this region. EPR measurements have shown an increase in the mobilisation of a spin-labelled side

Table 1. Overview of changes in interactions in helices G and F upon light activation

Region	Helix	Number of amino acids from the C-terminus	Number of amino acids from the N-terminus	Transducer binding	Light activation in receptor	Light activation in complex
1	G	31–37	208–214	−	−	
2	G	38–43	202–207	+	−	−
3	G	44–55	190–201	+		
4	G-F loop	56–67	178–189	+	+	−
5	F	68–93	177–152	+	+	
5A	F	71–77	168–174	+	+	−
5B	F	88–93	152–157	+	+	−

An increase in a region with interactions is indicated with (+), whereas a decrease in a region with interactions is indicated with (−).

chain between helices F and G upon light activation for *Np*SRII alone and in complex,[30] indicating an increase in the distance of helices G and F. In contradiction, the crystal structure of the light-activated receptor in its M state shows that helices F and G are stabilised by a hydrogen bond between Asp214 (helix G) and Arg162 (helix F).[29]

In all other regions in which light activation shows an effect on stability (regions 4, 5A and 5B), transducer binding causes the inversion of the observed effect. Light activation and transducer binding alone lead to an increase in stabilisation. Interestingly, light activation in the presence of the transducer reduces the strong stabilisation that has been induced by transducer binding. However, results from FRET and EPR measurements show a close proximity of the EF loop and transducer helix TM2, which is increased upon light activation.[26,28]

Force spectroscopy data reveal new locations of structural changes upon light excitation

The mechanism of signal transduction upon light activation, as generally discussed, includes isomerisation of the retinal, outward movement of the cytoplasmic half of helix F and clockwise rotation of the transducer helix TM2.[2] This model is based on FRET,[28] Fourier transform infrared[31] spectroscopy, EPR[26,30] spectroscopy, isothermal titration calorimetry[27] and molecular dynamics simulations.[32] However, a different structural rearrangement was found in the crystal structure of the excited state.[29]

After light absorption, the retinal isomerises, and the water cluster next to the retinal binding in the extracellular part of the channel is reorganised. This is likely to be the reason for the reduced stability observed in region 2; as expected, it is found both, in the presence and in the absence of the transducer.

The crystal structure revealed a hydrogen bond between Thr204 in region 2 and Tyr174 in helix F in region 5A that is described to be crucial for signalling.[33] Interestingly, in the complex, light activation strongly decreases the stability in region 5A, which harbours the retinal-binding pocket and is adjacent to region 2 (Fig. 3c). However, this decrease is not due to a loss of interaction with helix G, as this helix is already unfolded at this point of the measurement. While hardly any stable unfolding intermediates are observed in region 5 in *Np*SRII alone, transducer binding strongly stabilises this region. Thus, it is likely that the decrease observed in region 5A upon light activation is due to a weaker binding between this region of helix F and the transducer helix TM2. Other measurements revealed an increased dissociation constant of the light-activated protein complex,[34] which our data might assign to a weakening of binding in this region. We observe a similar decrease in stability in the loop regions of helix F (regions 4 and 5B). Since the crystal structure does not resolve any interactions between the cytoplasmic end of helix F and TM2, it is likely that the stabilisation we have observed upon complex formation is a result of intramolecular interactions that are induced by transducer binding. Intramolecular rearrangements upon light activation, as revealed by EPR measurements, might explain the decrease in interactions in region 5B, as observed in our experiment. Interestingly, in regions 4, 5A and 5B, we observe an inverse behaviour upon light activation when the transducer is absent; here, a slight increase indicating intramolecular stabilisation is found upon light activation. Destabilising effects are observed at the cytoplasmic half of helix G upon light activation (region 1) only in the absence of the transducer, but not in the complex. This might be responsible for the opening of the cytoplasmic cleft, which allows the proton-pumping activity of this protein.[35] That this effect is not observed when *Np*HtrII is bound might be another indication to explain its proton-pumping inhibition.[6,7,27]

The presented differences in intermolecular and intramolecular interactions, which depend on the presence of the transducer, highlight important regions in the protein that are responsible for the completely different response after light activation. Due to the analysed distributions being multimodal, standard histogram would give a low accuracy on the localisation of these differences. Only the application of average shifted histograms to force spectroscopic data allows us to increase the accuracy to a resolution of about six amino acids. However, some changes in peak occurrence probability are close to the estimated 1σ error limit of 68%. Interestingly, regions that have not been described before to show conformational changes upon light activation (regions 5A and 5B) are clearly above the error limits, while regions with changes close to the error limits point to conformational changes that have been described already with other biophysical methods. Most of the observed changes in stability are in good agreement with previously published results obtained with different biophysical methods. The additionally identified regions might be very interesting for further investigations using other techniques.

Experimental Procedures

Sample preparation

*Np*SRII and *Np*HtrII$_{114}$ from *N. pharaonis* were overexpressed as His-tagged proteins in *Escherichia coli* and purified by affinity chromatography using a Ni-NTA agarose column (QIAGEN, Hilden, Germany). *Np*SRII was then reconstituted into purple membrane lipids with a 1:35 (wt/wt) protein-to-lipid ratio.[36] *Np*SRII/*Np*HtrII$_{114}$ complexes were prepared by mixing *Np*SRII and *Np*HtrII$_{114}$ at a ratio of 1:1, followed by reconstitution into lipids.[14]

Force measurements

Force–distance measurements were performed in 20 mM Tris–HCl and 300 mM NaCl (pH 7.8) on membrane patches with reconstituted *Np*SRII or *Np*SRII/*Np*HtrII,

which were adsorbed on mica support. To activate the protein, we illuminated the sample with blue light using a high-intensity arc lamp with a filter of $\lambda = 460–500$ nm and 290 $\mu W/cm^2$.

The tip was pushed into the sample with a force of ~200 pN to allow coupling of the C-terminus of *Np*SRII (as previously described[15,18]) and was retracted with 400 nm/s. Cantilever deflection was recorded over the distance with a sampling rate of 33 kHz.

Si_3N_4 cantilevers (spring constant, 20 pN/nm; model OMCL TR400; Olympus) were used, and the spring constant was determined using the equipartition theorem.[37]

To couple the C-terminus to the tip, we took advantage of unspecific interactions. Since the C-terminus has 23 amino acids outside the membrane while the N-terminus is embedded in the membrane, the probability of attaching the tip to the N-terminal end is negligible. Thus, it is assured that we unfold only those *Np*SRII that are oriented with the C-terminus on the upper side.[17]

To include only those curves where *Np*SRII was attached with the terminus towards the tip, we selected the longest force curves (>60 nm) in accordance with the criteria described by Oesterhelt *et al.*[15] and Cisneros *et al.*[17] Under each condition (light/dark, presence/absence of HtrII), ~100 curves were taken into account for further analysis.

Data analysis

Selected force curves were analysed by fitting each force peak to the WLC model with a monomer length of 3.6 Å and a persistence length of 4.0 Å[15,38] using self-written procedures in IGOR.

The WLC model with a persistence length of 4 Å fits unfolded amino acid chains best above forces of 50 pN. At lower forces, as measured for the unfolding of the last helix, this model overestimates the chain length. However, this effect is negligible at the unfolding of helices G and F. To eliminate chain length variations that originate from a randomly varying anchoring point within the C-terminus, we aligned all curves by superposing on the second and third force peaks.

Acknowledgements

L.O. is a fellow of the North Rhine-Westphalia Research School BioStruct. This work was supported by grants from the Ministry of Innovation, Science, Research and Technology of the German Federal State North Rhine-Westphalia and from the Entrepreneur Foundation at the Heinrich-Heine-Universität Düsseldorf.

References

1. Sharma, A. K., Spudich, J. L. & Doolittle, W. F. (2006). Microbial rhodopsins: functional versatility and genetic mobility. *Trends Microbiol.* **14**, 463–469.
2. Klare, J. P., Chizhov, I. & Engelhard, M. (2008). Microbial rhodopsins: scaffolds for ion pumps, channels, and sensors. *Results Probl. Cell Differ.* **45**, 73–122.
3. Klare, J. P., Gordeliy, V. I., Labahn, J., Buldt, G., Steinhoff, H. -J. & Engelhard, M. (2004). The archaeal sensory rhodopsin II/transducer complex: a model for transmembrane signal transfer. *FEBS Lett.* **564**, 219–224.
4. Haupts, U., Tittor, J., Bamberg, E. & Oesterhelt, D. (1997). General concept for ion translocation by halobacterial retinal proteins: the isomerization/switch/transfer (IST) model. *Biochemistry*, **7**, 2–7.
5. Haupts, U., Tittor, J. & Oesterhelt, D. (1999). Closing in on bacteriorhodopsin: progress in understanding the molecule. *Annu. Rev. Biophys. Biomol. Struct.* **28**, 367–399.
6. Spudich, J. L. (1998). Variations on a molecular switch: transport and sensory signalling by archaeal rhodopsins. *Mol. Microbiol.* **28**, 1051–1058.
7. Schmies, G., Engelhard, M., Wood, P. G., Nagel, G. & Bamberg, E. (2001). Electrophysiological characterization of specific interactions between bacterial sensory rhodopsins and their transducers. *Proc. Natl Acad. Sci. USA*, **98**, 1555–1559.
8. Sudo, Y., Iwamoto, M., Shimono, K., Sumi, M. & Kamo, N. (2001). Photo-induced proton transport of pharaonis phoborhodopsin (sensory rhodopsin II) is ceased by association with the transducer. *Biophys. J.* **80**, 916–922.
9. Rudolph, J. & Oesterhelt, D. (1995). Chemotaxis and phototaxis require a CheA histidine kinase in the archaeon *Halobacterium salinarium*. *EMBO J.* **14**, 667–673.
10. Rudolph, J. & Oesterhelt, D. (1996). Deletion analysis of the che operon in the archaeon *Halobacterium salinarium*. *J. Mol. Biol.* **258**, 548–554.
11. Spudich, J. L. (2006). The multitalented microbial sensory rhodopsins. *Trends Microbiol.* **14**, 480–487.
12. Sudo, Y. & Spudich, J. L. (2006). Three strategically placed hydrogen-bonding residues convert a proton pump into a sensory receptor. *Proc. Natl Acad. Sci.* **103**, 16129–16134.
13. Spudich, J. L. & Luecke, H. (2002). Sensory rhodopsin II: functional insights from structure. *Curr. Opin. Struct. Biol.* **12**, 540–546.
14. Wegener, A. A., Klare, J. P., Engelhard, M. & Steinhoff, H. J. (2001). Structural insights into the early steps of receptor–transducer signal transfer in archaeal phototaxis. *EMBO J.* **20**, 5312–5319.
15. Oesterhelt, F., Oesterhelt, D., Pfeiffer, M., Engel, A., Gaub, H. E. & Müller, D. J. (2000). Unfolding pathways of individual bacteriorhodopsins. *Science*, **288**, 143–146.
16. Kedrov, A., Janovjak, H., Sapra, K. T. & Muller, D. J. (2007). Deciphering molecular interactions of native membrane proteins by single-molecule force spectroscopy. *Annu. Rev. Biophys. Biomol. Struct.* **36**, 233–260.
17. Cisneros, D. A., Oberbarnscheidt, L., Pannier, A., Klare, J. P., Helenius, J., Engelhard, M. *et al.* (2008). Transducer binding establishes localized interactions to tune sensory rhodopsin II. *Structure*, **16**, 1206–1213.
18. Muller, D. J., Kessler, M., Oesterhelt, F., Moller, C., Oesterhelt, D. & Gaub, H. (2002). Stability of bacteriorhodopsin alpha-helices and loops analyzed by single-molecule force spectroscopy. *Biophys. J.* **83**, 3578–3588.
19. Janovjak, H., Kedrov, A., Cisneros, D. A., Sapra, K. T., Struckmeier, J. & Muller, D. J. (2006). Imaging and detecting molecular interactions of single transmembrane proteins. *Neurobiol. Aging*, **27**, 546–561.
20. Gordeliy, V. I., Labahn, J., Moukhametzianov, R., Efremov, R., Granzin, J., Schlesinger, R. *et al.* (2002).

Molecular basis of transmembrane signalling by sensory rhodopsin II–transducer complex. *Nature*, **419**, 484–487.
21. Scott, D. (1992). *Multivariate Density Estimation.* John Wiley, New York.
22. Scott, D. W. (1979). On optimal and data-based histograms. *Biometrika*, **66**, 605–610.
23. Freedman, D. & Diaconis, P. (1981). On the histogram as a density estimator: L2 theory. *Z. Wahrscheinlichkeitstheor. Verw. Geb.* **57**, 453–476.
24. Izenman, A. J. (1991). Recent development in nonparametric density estimation. *J. Am. Stat. Assoc.* **86**, 205–224.
25. Klare, J. P., Bordignon, E., Doebber, M., Fitter, J., Kriegsmann, J., Chizhov, I. *et al.* (2006). Effects of solubilization on the structure and function of the sensory rhodopsin II/transducer complex. *J. Mol. Biol.* **356**, 1207–1221.
26. Wegener, A. -A., Chizhov, I., Engelhard, M. & Steinhoff, H. -J. (2000). Time-resolved detection of transient movement of helix F in spin-labelled pharaonis sensory rhodopsin II. *J. Mol. Biol.* **301**, 881–891.
27. Hippler-Mreyen, S., Klare, J. P., Wegener, A. A., Seidel, R., Herrmann, C., Schmies, G. *et al.* (2003). Probing the sensory rhodopsin II binding domain of its cognate transducer by calorimetry and electrophysiology. *J. Mol. Biol.* **330**, 1203–1213.
28. Yang, C. -S., Sineshchekov, O., Spudich, E. N. & Spudich, J. L. (2004). The cytoplasmic membrane-proximal domain of the HtrII transducer interacts with the E-F loop of photoactivated *Natronomonas pharaonis* sensory rhodopsin II. *J. Biol. Chem.* **279**, 42970–42976.
29. Moukhametzianov, R., Klare, J. P., Efremov, R., Baeken, C., Göppner, A., Labahn, J. *et al.* (2006). Development of the signal in sensory rhodopsin and its transfer to the cognate transducer. *Nature*, **440**, 115–119.
30. Bordignon, E., Klare, J. P., Holterhues, J., Martell, S., Krasnaberski, A., Engelhard, M. & Steinhoff, H. -J. (2007). Analysis of light-induced conformational changes of *Natronomonas pharaonis* sensory rhodopsin II by time resolved electron paramagnetic resonance spectroscopy. *Photochem. Photobiol.* **83**, 263–272.
31. Kamada, K., Furutani, Y., Sudo, Y., Kamo, N. & Kandori, H. (2006). Temperature-dependent interactions between photoactivated pharaonis phoborhodopsin and its transducer. *Biochemistry*, **45**, 4859–4866.
32. Inoue, K., Sasaki, J., Spudich, J. L. & Terazima, M. (2008). Signal transmission through the HtrII transducer alters the interaction of two alpha-helices in the HAMP domain. *J. Mol. Biol.* **29**, 963–970.
33. Sudo, Y., Furutani, Y., Kandori, H. & Spudich, J. L. (2006). Functional importance of the interhelical hydrogen bond between Thr204 and Tyr174 of sensory rhodopsin II and its alteration during the signaling process. *J. Biol. Chem.* **281**, 34239–34245.
34. Sudo, Y., Iwamoto, M., Shimono, K. & Kamo, N. (2001). Pharaonis phoborhodopsin binds to its cognate truncated transducer even in the presence of a detergent with a 1:1 stoichiometry. *Photochem. Photobiol.* **74**, 489–494.
35. Schmies, G., Luttenberg, B., Chizhov, I., Engelhard, M., Becker, A. & Bamberg, E. (2000). Sensory rhodopsin II from the haloalkaliphilic *Natronobacterium pharaonis*: light-activated proton transfer reactions. *Biophys. J.* **78**, 967–976.
36. Hohenfeld, I. P., Wegener, A. A. & Engelhard, M. (1999). Purification of histidine tagged bacteriorhodopsin, pharaonis halorhodopsin and pharaonis sensory rhodopsin II functionally expressed in *Escherichia coli*. *FEBS Lett.* **442**, 198–202.
37. Butt, H. J., Jaschke, M. & Ducker, W. (1995). Measuring surface forces in aqueous electrolyte solution with the atomic force microscope. *Bioelectrochem. Bioenerg.* **38**, 191–201.
38. Rief, M., Gautel, M., Oesterhelt, F., Fernandez, J. M. & Gaub, H. E. (1997). Reversible unfolding of individual titin immunoglobulin domains by AFM. *Science*, **276**, 1109–1112.